Supporting Information

Aerobic Melt-Quenching and Glass Formation in One-Dimensional Metal–Organic Hybrids

Shruti Kirti,[a] Patrick Schlachta,[b] Sebastian A. Hallweger,[b] Gregor Kieslich,[b] Christoph Hartmann,[c] Bikash Kumar Shaw [a,b]*

[a] Department of Chemistry, Indian Institute of Technology (BHU), Varanasi 221 005, India.

[b] Department of Chemistry, Technical University of Munich, Garching 85748, Germany.

[c] Chair of Metal Forming and Casting, Technical University of Munich, Garching 85748, Germany.

Synthesis

Reagents:

$Mn(NO_3)_2 \cdot 4H_2O$ (98.5%, Sigma-Aldrich), $FeCl_2$ (98%, Sigma-Aldrich), $Co(NO_3)_2 \cdot 6H_2O$ (98%, Sigma-Aldrich), $Ni(NO_3)_2 \cdot 6H_2O$ (98%, Sigma-Aldrich), $Cu(NO_3)_2 \cdot 6H_2O$ (98%, Sigma-Aldrich), $(PrPh_3P)Br$ (98%, Aldrich), and Na(dca) (96%, Sigma-Aldrich) were purchased as indicated and used as received.

Procedure:

$(PrPh_3P)_2[M(dca)_4]$ (M = Mn, Fe, Co, Ni, Cu) materials were synthesized by solvent layering method. Typically, 10 mL of an aqueous solution of the metal salts (2 mmol) (0.502 g of $Mn(NO_3)_2.4H_2O$, 0.254 g of $FeCl_2 \cdot 4H_2O$, 0.582 g of $Co(NO_3)_2 \cdot 6H_2O$, 0.584 g of $Ni(NO_3)_2 \cdot 6H_2O$, 0.480 g of $Cu(NO_3)_2 \cdot 6H_2O$) were placed at the bottom of a thin crystallization tube, and layered with a mixture of a sodium dicyanamide solution in 10 mL of water (0.712 g, 8 mmol) and the propyltriphenylphosphonium (1.54 g, 4 mmol) solution in 10 mL of ethanol respectively. Block-shaped single crystals were isolated from the mother liquor after one week of slow evaporation in an open atmosphere at 298 K.

Single-crystal X-ray diffraction

SC-XRD data were collected on a Bruker D8-Venture single crystal x-ray diffractometer equipped with an IMS microsource with MoKα radiation (λ = 0.71073 Å), a Bruker Photon III detector and a Helios optic, using the Bruker APEX4 software package.[1] Single crystals were fixed on top of a micro sampler and frozen under a stream of cold nitrogen. A matrix scan was used to determine the initial lattice parameters. All data were integrated with the Bruker SAINT V8.40B software package using a narrow-frame algorithm and the reflections were corrected for Lorentz and polarization effects, scan speed, and background.[2] Data were corrected for absorption effects including odd and even ordered spherical harmonics by the multi-scan method (SADABS 2016/2).[3] Space group assignment was based upon systematic absences, E statistics, and successful refinement of the structure.
The structures were solved by direct methods using SHELXT and refined by full-matrix least-squares methods against F^2 by minimizing $\Sigma w(F_o^2 - F_c^2)^2$ using SHELXL in conjunction with SHELXLE.[4-6] All non-hydrogen atoms were refined with anisotropic displacement parameters. Hydrogen atoms were refined isotropically on calculated positions using a riding model with their U_{iso} values constrained to 1.5 times the U_{eq} of their pivot atoms for terminal sp^3 carbon atoms and a C–H distance of 0.98 Å. Non-methyl hydrogen atoms were refined using a riding model with aromatic, and other C–H distances of 0.95 Å, and 1.00 Å, respectively, and U_{iso} values constrained to 1.2 times the U_{eq} of their pivot atoms. Neutral atom scattering factors for all atoms and anomalous dispersion corrections for the non-hydrogen atoms were taken from International Tables for Crystallography.[7] Crystallographic data for the structures reported in this paper have been deposited with the Cambridge Crystallographic Data Centre.[8] Supplementary crystallographic data reported in this paper have been deposited with the Cambridge Crystallographic Data Centre (CCDC 2480284-2480288) and can be obtained free of charge from The Cambridge Crystallographic Data Centre via www.ccdc.cam.ac.uk/structures. Images of the crystal structures were generated with Mercury and Vesta.

Magnetic Measurements

The temperature variation of field-cooled susceptibility (*M-T*) data was collected at 100 Oe magnetic field at a temperature range 2 – 300 K. Samples were placed in a lightweight homogeneous quartz tube to minimize the background noise and stray field effects. The magnetic data were corrected for the diamagnetic contribution from the quartz sample holder and the intrinsic diamagnetism of the samples by the standard literature using Pascal's constants.

Table S1. Crystal data and structure refinement details for $(PrPh_3P)_2[M(dca)_4]$ (M = Mn, Fe, Co, Ni, Cu).

	$(PrPh_3P)_2[Mn(dca)_4]$	$(PrPh_3P)_2[Fe(dca)_4]$	$(PrPh_3P)_2[Co(dca)_4]$	$(PrPh_3P)_2[Ni(dca)_4]$	$(PrPh_3P)_2[Cu(dca)_4]$
CCDC number	2480284	2480285	2480286	2480287	2480288
Empirical formula	$C_{50}H_{44}Mn_1N_{12}P_2$	$C_{50}H_{44}Fe_1N_{12}P_2$	$C_{50}H_{44}Co_1N_{12}P_2$	$C_{50}H_{44}Ni_1N_{12}P_2$	$C_{50}H_{44}Cu_1N_{12}P_2$
Formula weight	925.82	930.76	933.84	933.62	938.45
Temperature/ K	100(2)	100(2)	100(2)	100(2)	100(2)
Crystal system	monoclinic	monoclinic	monoclinic	monoclinic	Monoclinic
Space group	$P2_1/n$	$P2_1/n$	$P2_1/n$	$P2_1/n$	$P2_1/n$
a/Å	15.557(6)	15.4288(7)	15.4178(9)	15.4003(7)	15.3571(11)
b/Å	7.499(2)	7.3833(3)	7.3443(4)	7.3129(3)	7.2877(6)
c/Å	21.216(8)	21.1645(9)	21.1830(12)	21.2075(10)	21.1224(15)
α/°	90	90	90	90	90
β/°	102.519(14)	103.184(2)	103.242(2)	103.394(2)	102.040(2)
γ/°	90	90	90	90	90
Volume/Å^3	2416.2(15)	2347.42(18)	2334.8(2)	2323.44(18)	2312.0(3)
Z	2	2	2	2	2
ρ_{calc} g/cm^3	1.273	1.317	1.328	1.334	1.348
μ/mm^{-1}	0.387	0.439	0.485	0.536	0.591
F(000)	958.0	968.0	970.0	972.0	974.0
Crystal size/mm^3	0.489 × 0.376 × 0.255	0.333 × 0.227 × 0.167	0.656 × 0.450 × 0.288	0.564 × 0.356 × 0.215	0.665 × 0.346 × 0.216
Crystal colour	colourless	colourless	purple	blue	Blue
Crystal shape	fragment	fragment	fragment	fragment	Fragment
Radiation	MoKα (λ = 0.71073)	MoKα (λ = 0.71073)	MoKα (λ = 0.71073)	MoKα (λ = 0.71073)	MoKα (λ = 0.71073)
2Θ range for data collec/°	3.934 to 54.18	3.954 to 54.966	3.95 to 56.598	3.95 to 55.74	3.94 to 56.61
Index ranges	$-19 \le h \le 19$, $-9 \le k \le 9$, $-27 \le l \le 27$	$-20 \le h \le 20$, $-9 \le k \le 9$, $-27 \le l \le 27$	$-20 \le h \le 20$, $-9 \le k \le 9$, $-28 \le l \le 28$	$-20 \le h \le 20$, $-9 \le k \le 9$, $-27 \le l \le 27$	$-20 \le h \le 20$, $-9 \le k \le 9$, $-28 \le l \le 28$
Reflections collected	116479	136417	141500	148907	88420
Independent reflections	5326 [R_{int} = 0.0693, R_{sigma} = 0.0229]	5376 [R_{int} = 0.0508, R_{sigma} = 0.0136]	5811 [R_{int} = 0.0337, R_{sigma} = 0.0098]	5540 [R_{int} = 0.0420, R_{sigma} = 0.0112]	5763 [R_{int} = 0.0378, R_{sigma} = 0.0142]
Data/restraints /parameters	5326/40/319	5376/0/297	5811/0/296	5540/0/296	5763/0/296
Goodness-of-fit (GooF) on F^2	1.198	1.168	1.145	1.116	1.209
Final R indexes [I≥2σ (I)]	R_1 = 0.0539, wR_2 = 0.1358	R_1 = 0.0570, wR_2 = 0.1264	R_1 = 0.0474, wR_2 = 0.0955	R_1 = 0.0525, wR_2 = 0.1177	R_1 = 0.0421, wR_2 = 0.0837
Final R indexes [all]	R_1 = 0.0789, wR_2 = 0.1672	R_1 = 0.0774, wR_2 = 0.1519	R_1 = 0.0600, wR_2 = 0.1083	R_1 = 0.0677, wR_2 = 0.1364	R_1 = 0.0588, wR_2 = 0.0975
Largest diff. peak/hole eÅ^{-3}	0.65/-0.41	1.125/-0.58	0.875/-0.54	1.026/-0.62	1.003/-0.54

$$R_1 = \sum\big||F_O| - |F_C|\big| \,/\, \sum|F_O|;\ wR_2 = [\,\sum w(F_O^2 - F_C^2)^2 \,/\, \sum w(F_O^2)^2\,]^{1/2};\ GooF = \big[\sum w(F_O^2 - F_C^2)^2 \,/\, (N_{ref} - N_{par})\,\big]^{1/2}$$

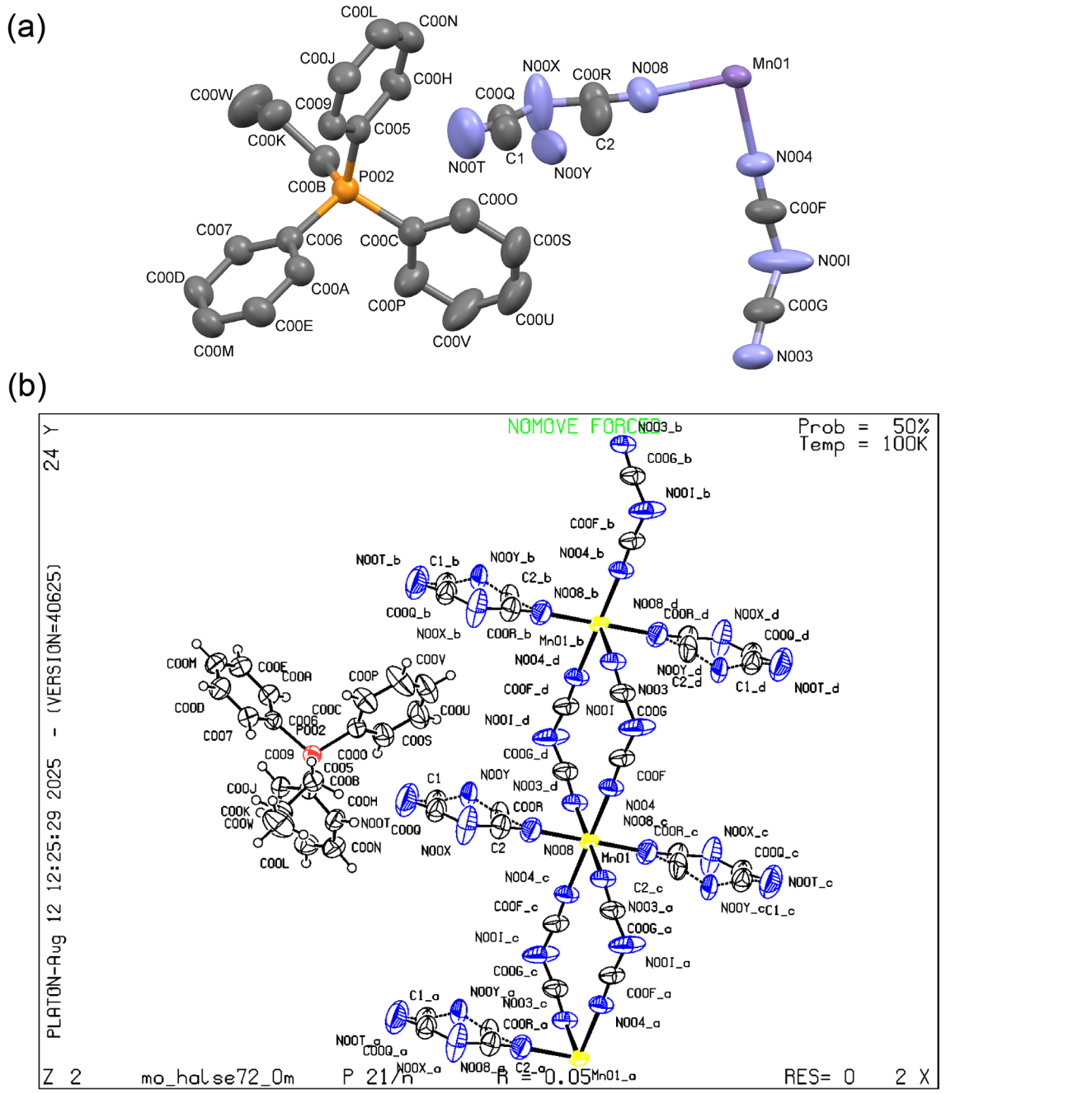

Figure S1. (a) Graphical representation using thermal ellipsoids of the asymmetric unit of $(PrPh_3P)_2[Mn(dca)_4]$ integrated by one PC_{21} structural unit at the site A and one MnN_6C_4 structural unit at the site B. The anionic molecular unit (axial positions) at site B exhibits positional disorder. All hydrogen atoms are omitted for clarity. **(b)** ORTEP view of the $(PrPh_3P)_2[Mn(dca)_4]$ molecular unit obtained from CheckCIF report. The positional disorder (axial positions) at site B is clearly revealed from this diagram.

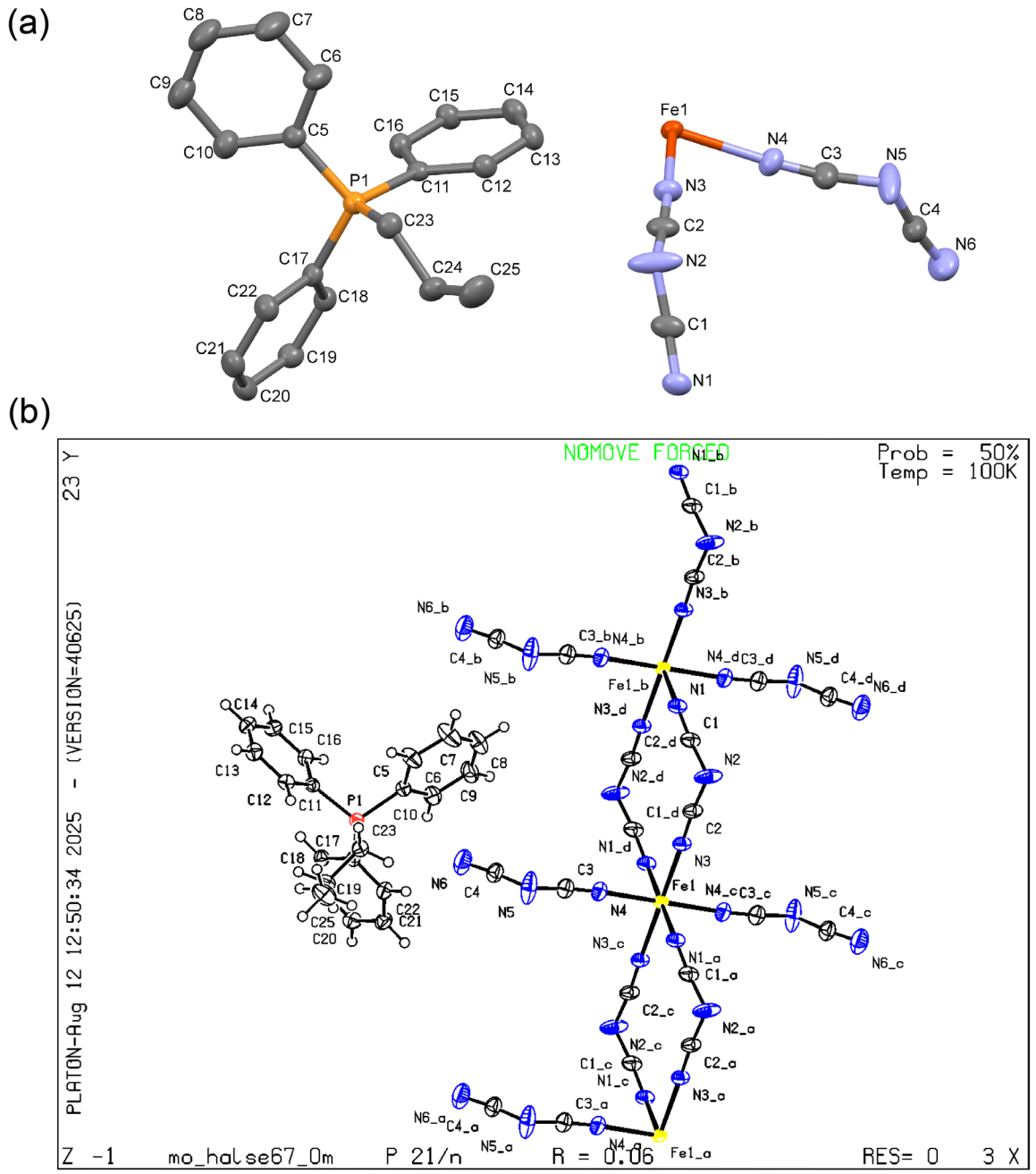

Figure S2. (a) Graphical representation using thermal ellipsoids of the asymmetric unit of $(PrPh_3P)_2[Fe(dca)_4]$ integrated by one PC_{21} structural unit at the site A and one FeN_6C_4 structural unit at the site B. The center nitrogen atoms of the dca linker at site B exhibits slight disorder. All hydrogen atoms are omitted for clarity. **(b)** ORTEP view of the $(PrPh_3P)_2[Fe(dca)_4]$ molecular unit obtained from CheckCIF report.

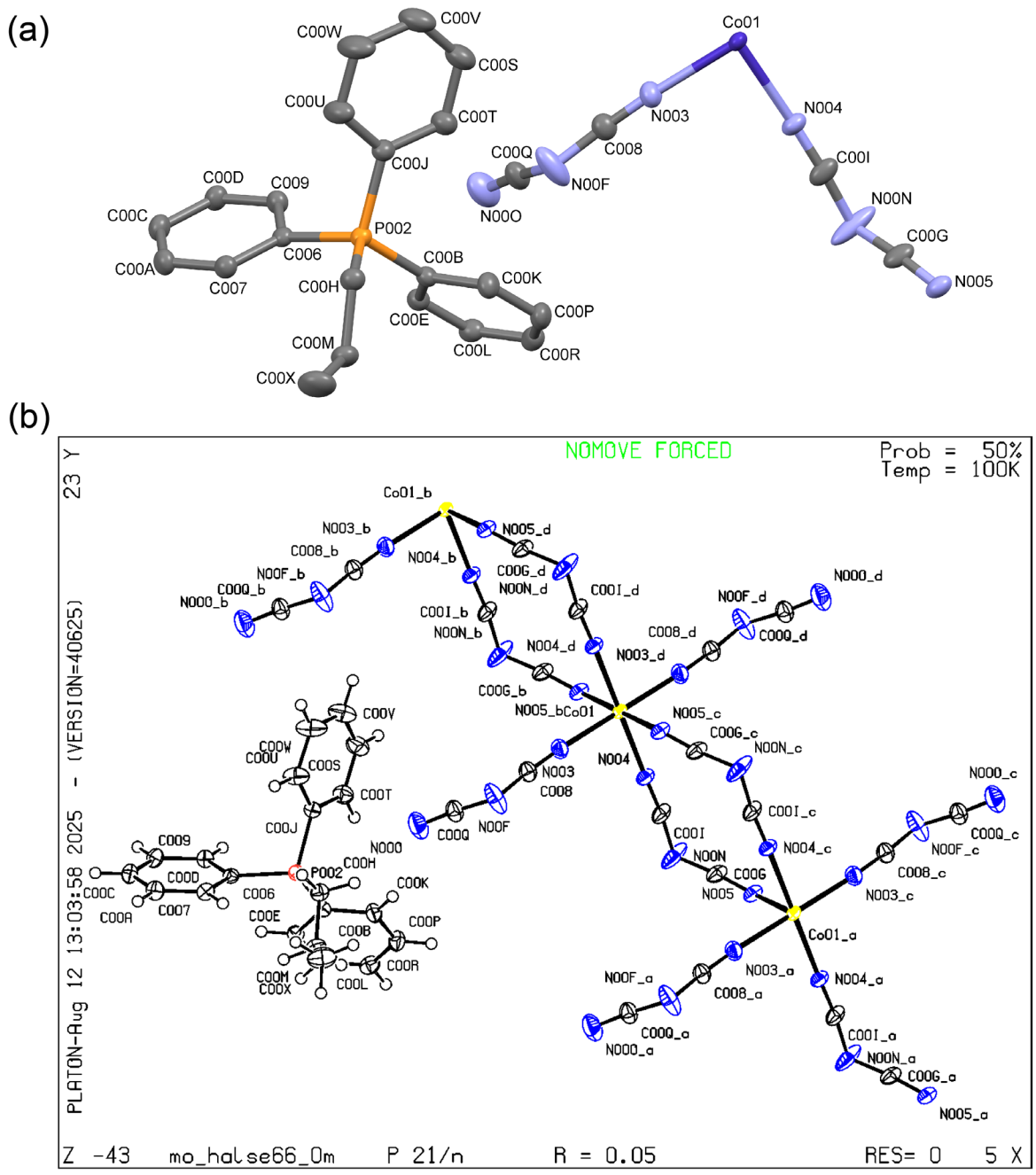

Figure S3. (a) Graphical representation using thermal ellipsoids of the asymmetric unit of $(PrPh_3P)_2[Co(dca)_4]$ integrated by one PC_{21} structural unit at the site A and one CoN_6C_4 structural unit at the site B. The center nitrogen atoms of the dca linker at site B exhibits slight disorder. All hydrogen atoms are omitted for clarity. **(b)** ORTEP view of the $(PrPh_3P)_2[Co(dca)_4]$ molecular unit obtained from CheckCIF report.

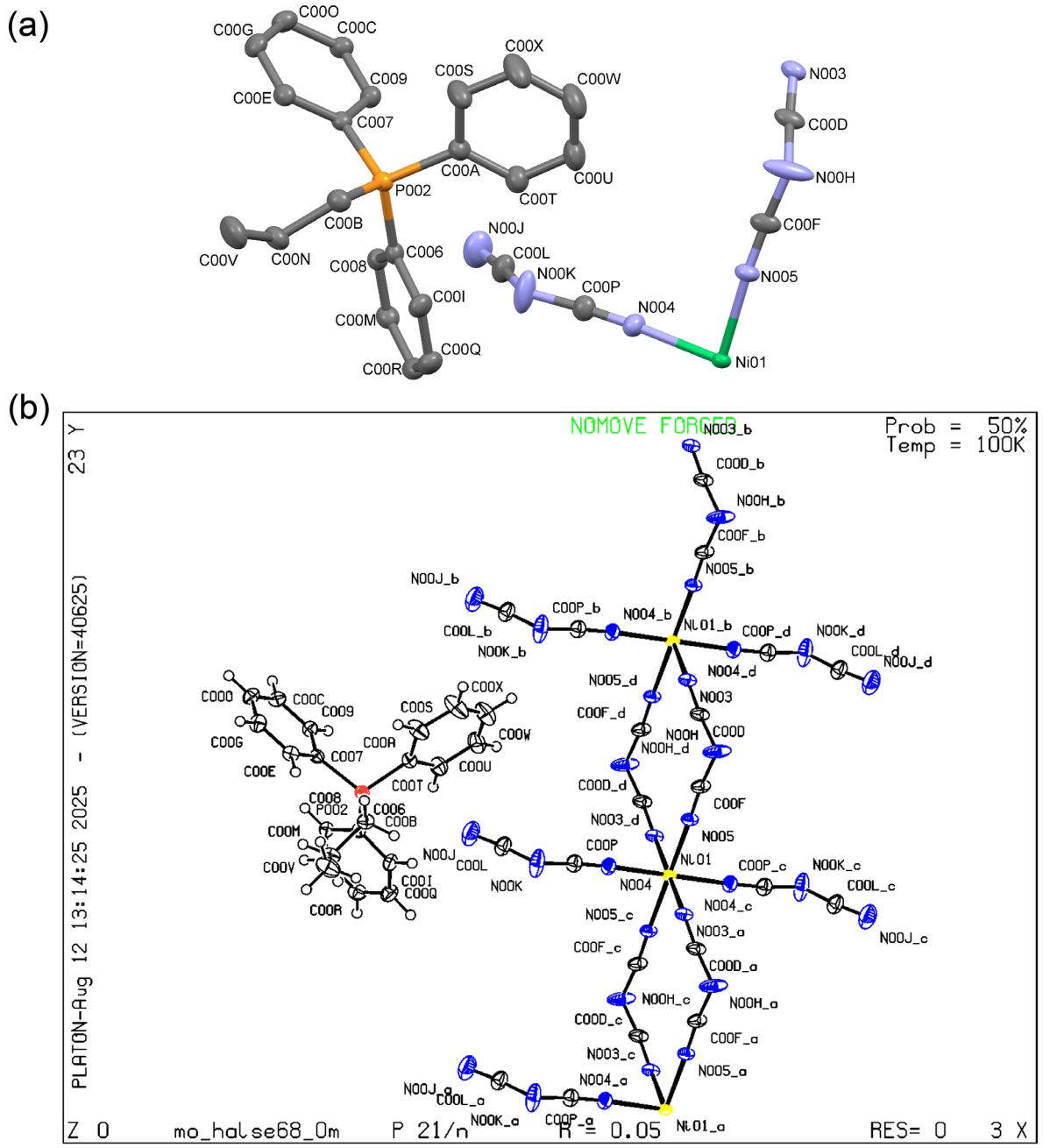

Figure S4. (a) Graphical representation using thermal ellipsoids of the asymmetric unit of $(PrPh_3P)_2[Ni(dca)_4]$ integrated by one PC_{21} structural unit at the site A and one NiN_6C_4 structural unit at the site B. The center nitrogen atoms of the dca linker at site B exhibits slight disorder. All hydrogen atoms are omitted for clarity. **(b)** ORTEP view of the $(PrPh_3P)_2[Ni(dca)_4]$ molecular unit obtained from CheckCIF report.

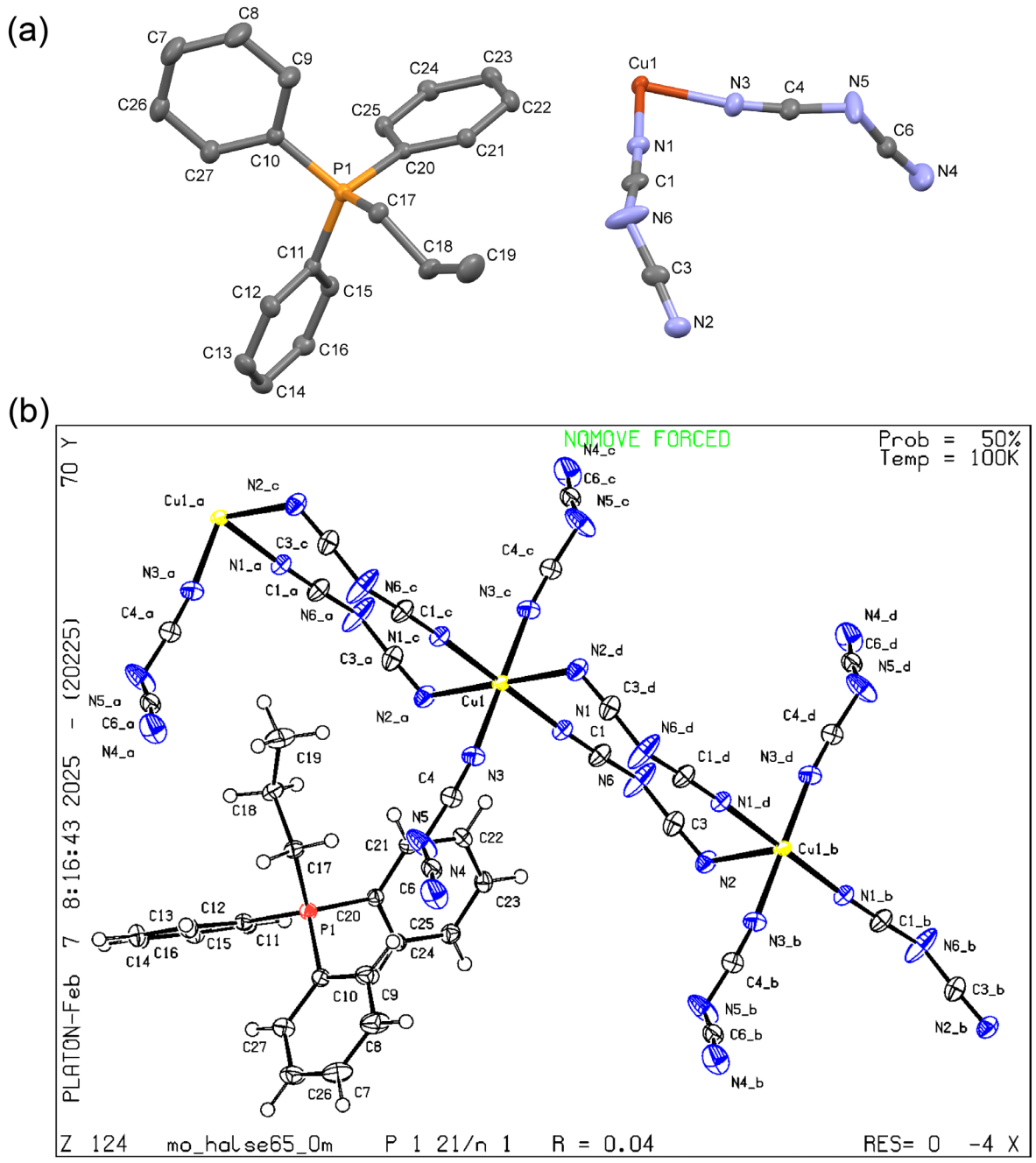

Figure S5. (a) Graphical representation using thermal ellipsoids of the asymmetric unit of $(PrPh_3P)_2[Cu(dca)_4]$ integrated by one PC_{21} structural unit at the site A and one CuN_6C_4 structural unit at the site B. The center nitrogen atoms of the dca linker at site B exhibits slight disorder. All hydrogen atoms are omitted for clarity. **(b)** ORTEP view of the $(PrPh_3P)_2[Cu(dca)_4]$ molecular unit obtained from CheckCIF report.

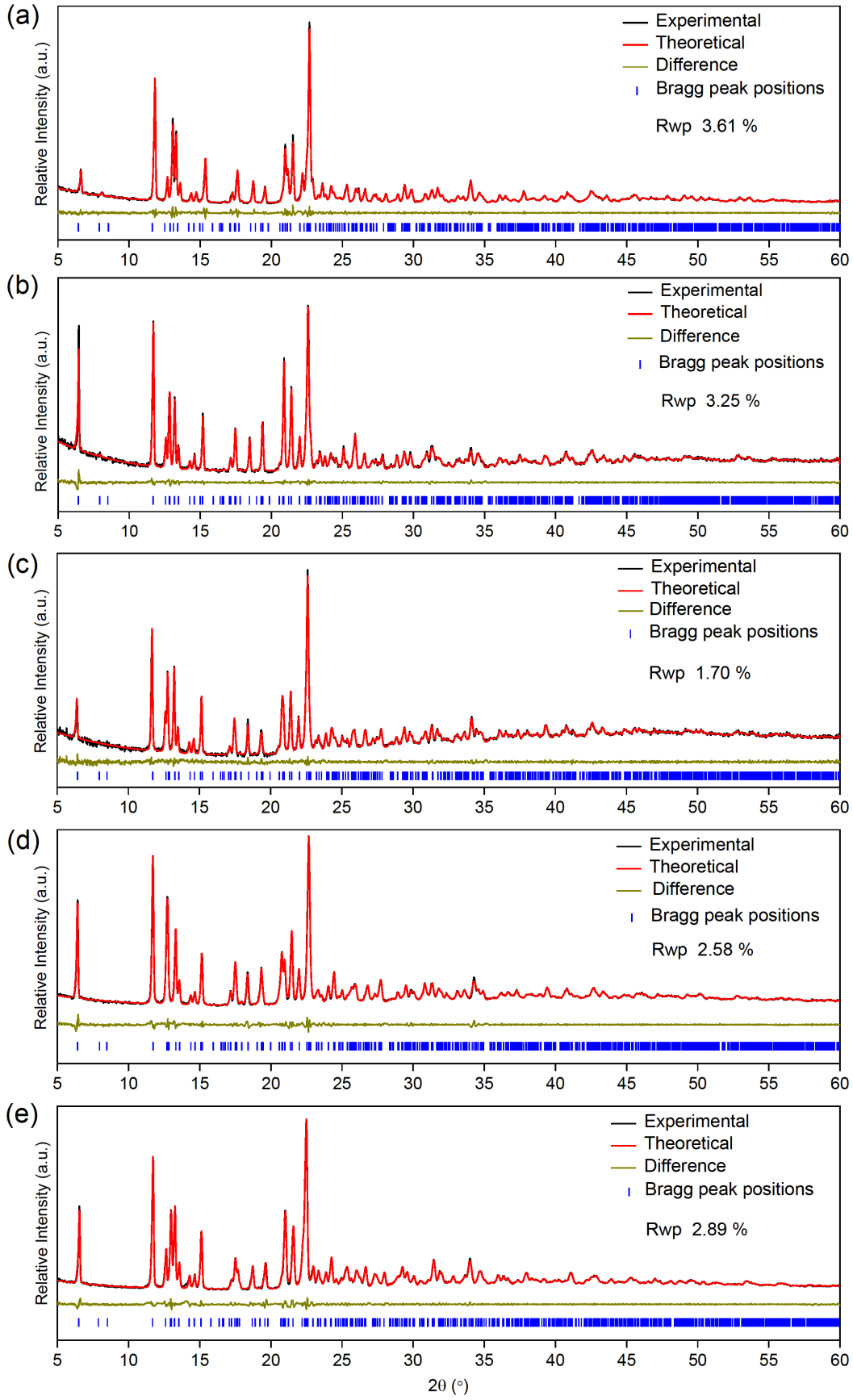

Figure S6: Pawley refinement of X-ray powder diffraction data using TOPAS academic v6 software. **(a) $(PrPh_3P)_2[Mn(dca)_4]$**, Experimental cell parameters (Å): a = 15.557(6), b =

7.499(2), *c* = 21.216(8), α = γ = 90°, β = 102.519(14)°; Refined cell parameters (Å): *a* = 15.5630(11), *b* = 7.5187(5), *c* = 21.1880(15), α = γ = 90°, β = 102.371(3)°. (**b**) **$(PrPh_3P)_2[Fe(dca)_4]$**, Experimental cell parameters (Å): *a* = 15.4288(7), *b* = 7.3833(3), *c* = 21.1645(9), α = γ = 90°, β = 103.184(2)°; Refined cell parameters (Å) *a* = 15.5132(17), *b* = 7.4817(8), *c* = 21.294(2), α = γ = 90°, β = 102.619(5)°. (**c**) **$(PrPh_3P)_2[Co(dca)_4]$**, Experimental cell parameters (Å): *a* = 15.4178(9), *b* = 7.3443(4), *c* = 21.1830(12), α = γ = 90°, β = 103.242(2)°; Refined cell parameters (Å): *a* = 15.4745(15), *b* = 7.4282(7), *c* = 21.3085(19), α = γ = 90°, β = 102.770(5)°. (**d**) **$(PrPh_3P)_2[Ni(dca)_4]$**, Experimental cell parameters (Å): *a* = 15.4003(7), *b* = 7.3129(3), *c* = 21.2075(10), α = γ = 90°, β = 103.394(2)°; Refined cell parameters (Å): *a* = 15.4709(16), *b* = 7.3928(7), *c* = 21.389(2), α = γ = 90°, β = 102.874(5)°. (**e**) **$(PrPh_3P)_2[Cu(dca)_4]$**, Experimental cell parameters (Å): *a* = 15.3571(11), *b* = 7.2877(6), *c* = 21.1224(15), α = γ = 90°, β = 102.040(2)°; Refined cell parameters (Å): *a* = 15.4491(12), *b* = 7.4561(6), *c* = 21.1781(16), α = γ = 90°, β = 101.478(4)°.

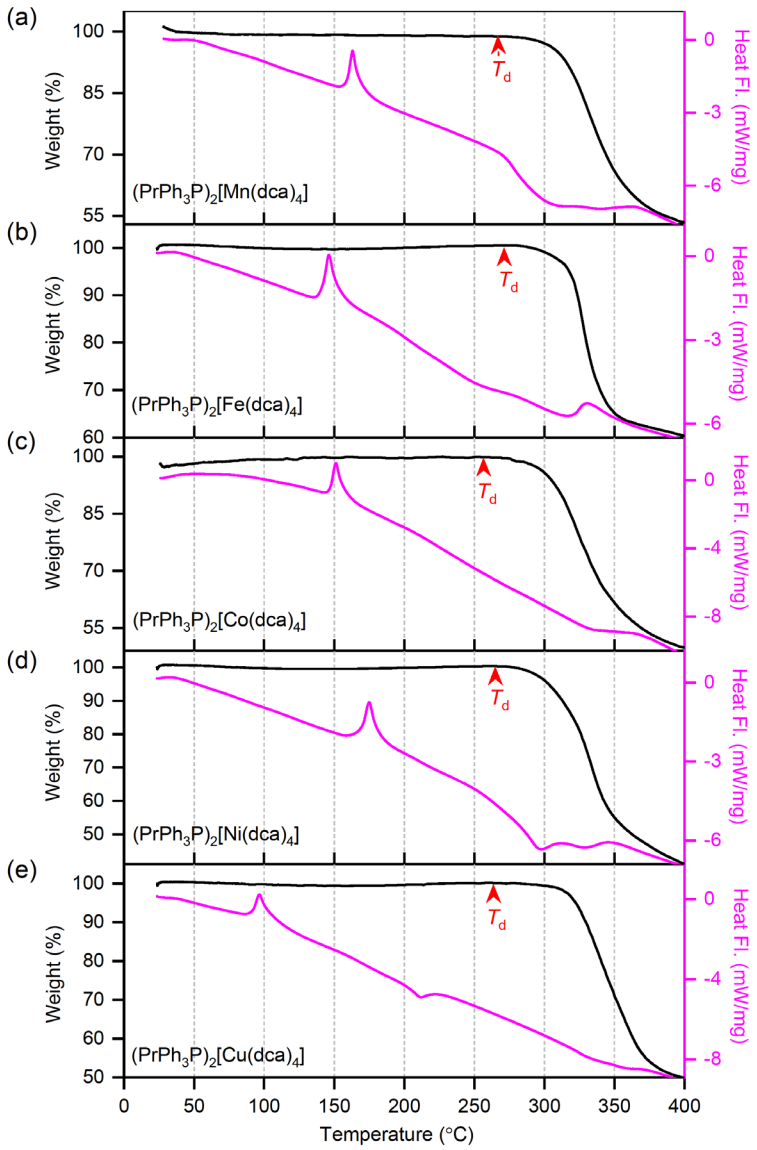

Figure S7. Change in weight % (black line, left axis) and corresponding change in heat flow (pink line, right axis) with temperature for **(a)** - **(e)** $(PrPh_3P)_2[M(dca)_4]$ (where M = Mn, Fe, Co, Ni, Cu), measured at a rate of 10 °C min^{-1} under Argon atmosphere. The absence of any mass loss at temperatures corresponding to the endotherms are indicative of melting in each case. The arrowheads (in red) represent the temperature at which decomposition (T_d) follows (265 °C for $(PrPh_3P)_2[Mn(dca)_4]$, 270 °C for $(PrPh_3P)_2[Fe(dca)_4]$, 255 °C for $(PrPh_3P)_2[Co(dca)_4]$, 265 °C for $(PrPh_3P)_2[Ni(dca)_4]$, 262 °C for $(PrPh_3P)_2[Cu(dca)_4]$).

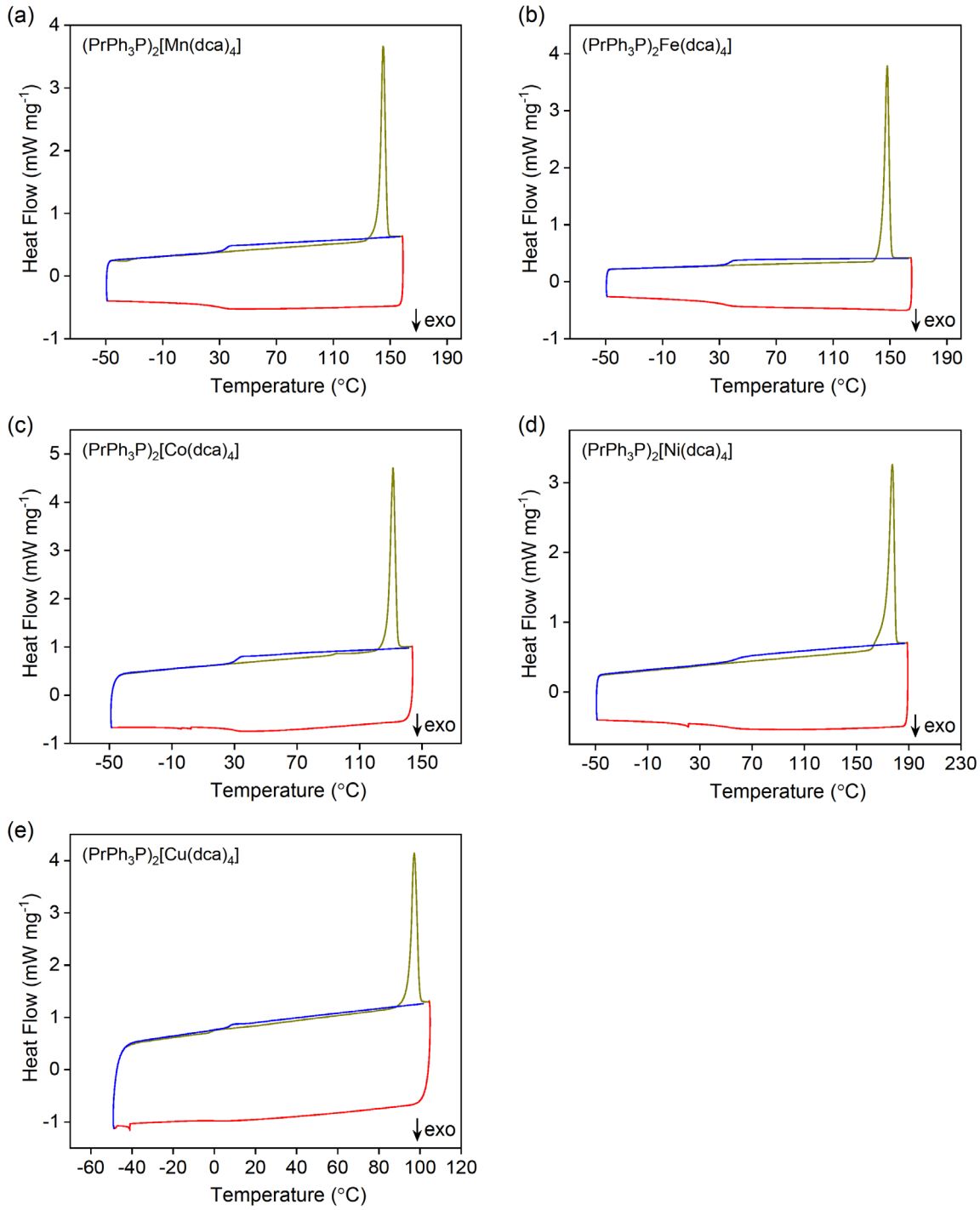

Figure S8: Change in heat flow as a function of temperature for **(a)** - **(e)** $(PrPh_3P)_2[M(dca)_4]$ (where M = Mn, Fe, Co, Ni, Cu). Crystals were first heated (dark yellow) +5 °C above T_m and then cooled (red) to -50 °C at a rate of 10 °C min^{-1}. The glass formed after quenching was then reheated (blue) at the same heating rate of 10 °C min^{-1} to obtain the glass transition (T_g) which was identified by the upraise in the heat flow and marked with black dashed box. The experiment was carried out in DSC Q2000 instrument.

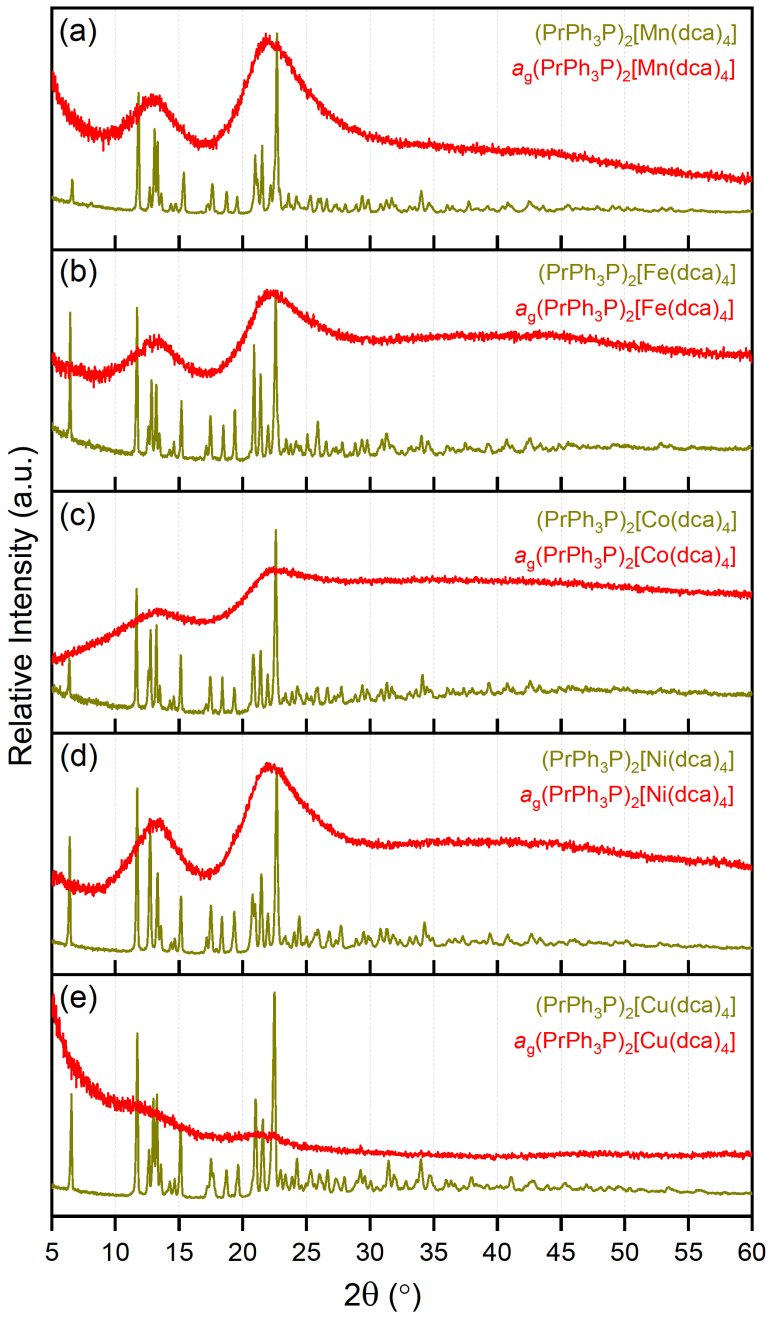

Figure S9: Ambient temperature powder X-ray diffraction patterns of **(a)** - **(e)** $(PrPh_3P)_2[M(dca)_4]$ (where M = Mn, Fe, Co, Ni, Cu), before heating (crystal, dark yellow) and upon quenching from the liquid phase (glass, red). These samples correspond to the glasses shown in **Figure 1(b-right)** prepared using the DSC technique.

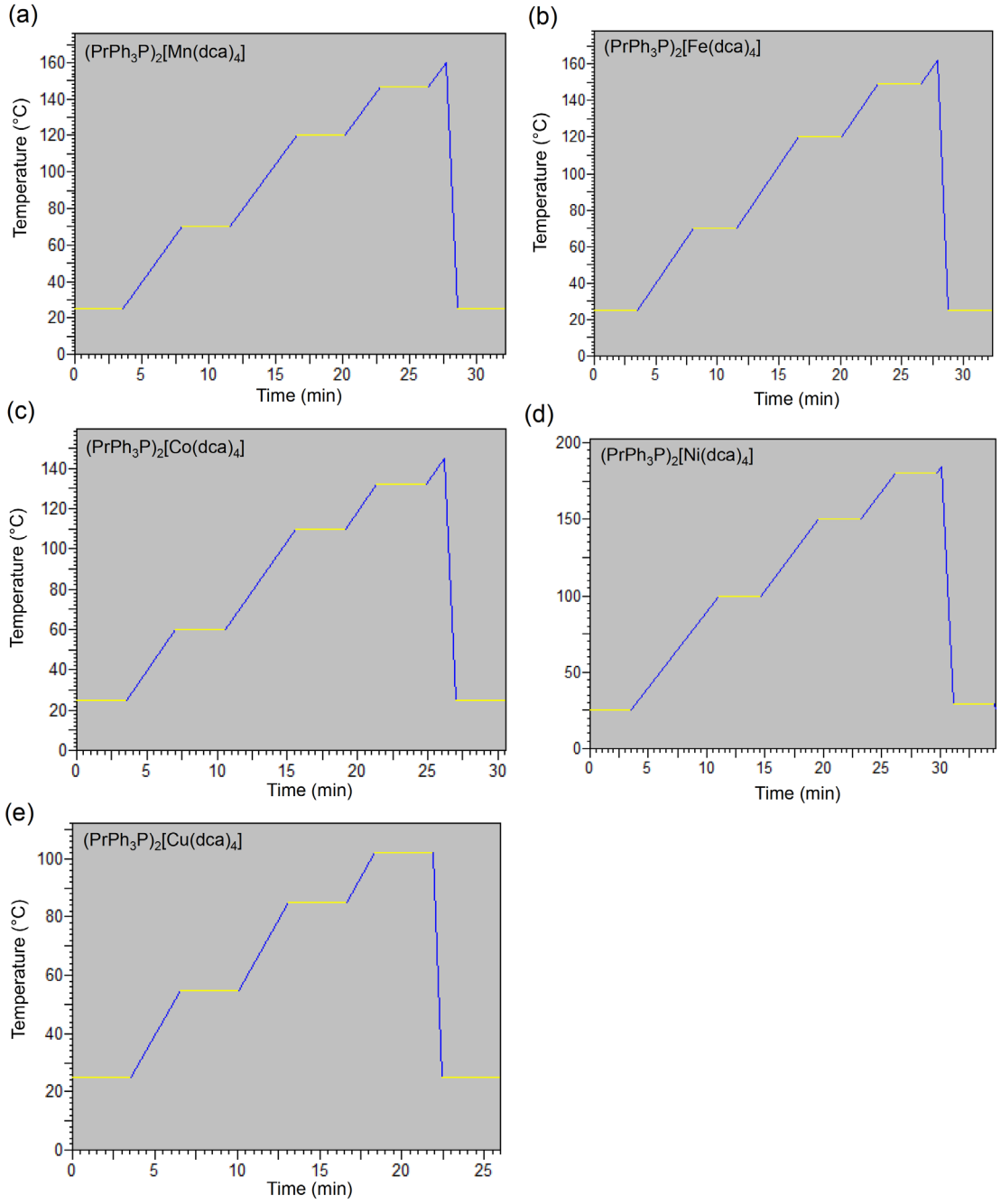

Figure S10. Temperature-Time profiles of variable temperature PXRD experiment for crystalline **(a) - (e)** $(PrPh_3P)_2[M(dca)_4]$ (where M = Mn, Fe, Co, Ni, Cu). Yellow lines represent 2θ scans from 5° – 30° (step size of 0.02° at a rate of 10° min^{-1}). During the heating scans (blue lines), a heating rate of 10 (±1) °C min^{-1} was applied. To comply with the DSC measurements, the maximum instrumental cooling (blue lines) was applied which provides a rate of 9 (±1) °C min^{-1}.

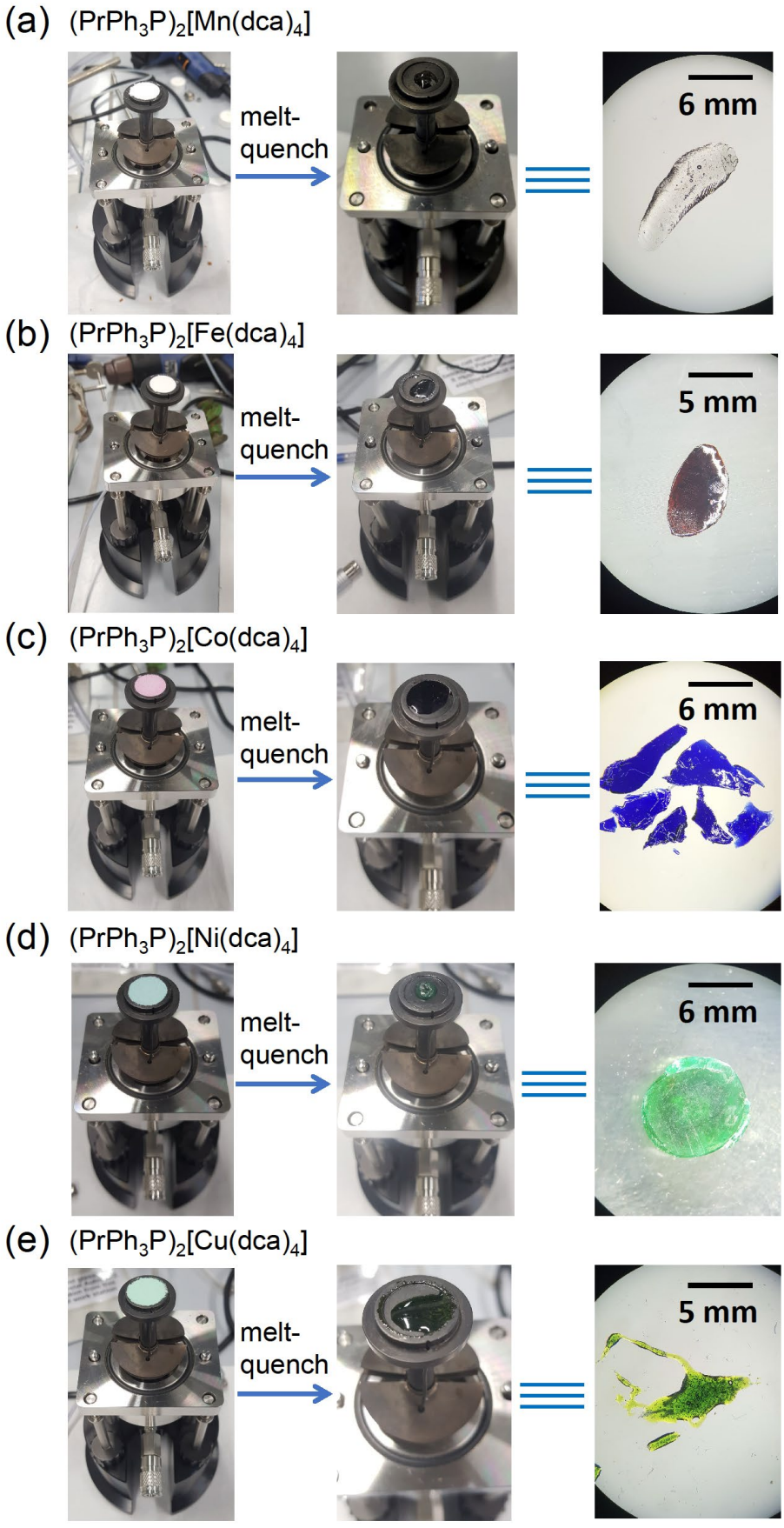

Figure S11. Optical images taken during variable temperature PXRD experiment for **(a)** - **(e)** $(PrPh_3P)_2[M(dca)_4]$ (where M = Mn, Fe, Co, Ni, Cu). Ground crystalline powder (~ 200 mg)

was placed on the Anton Paar sample holder (diameter 14 mm, thickness 0.8 mm). The second image was obtained after melt-quenching the sample which reveal flow like appearance due to liquification at high temperature. The glass pieces isolated from the sample holder were put under the optical microscope at third images.

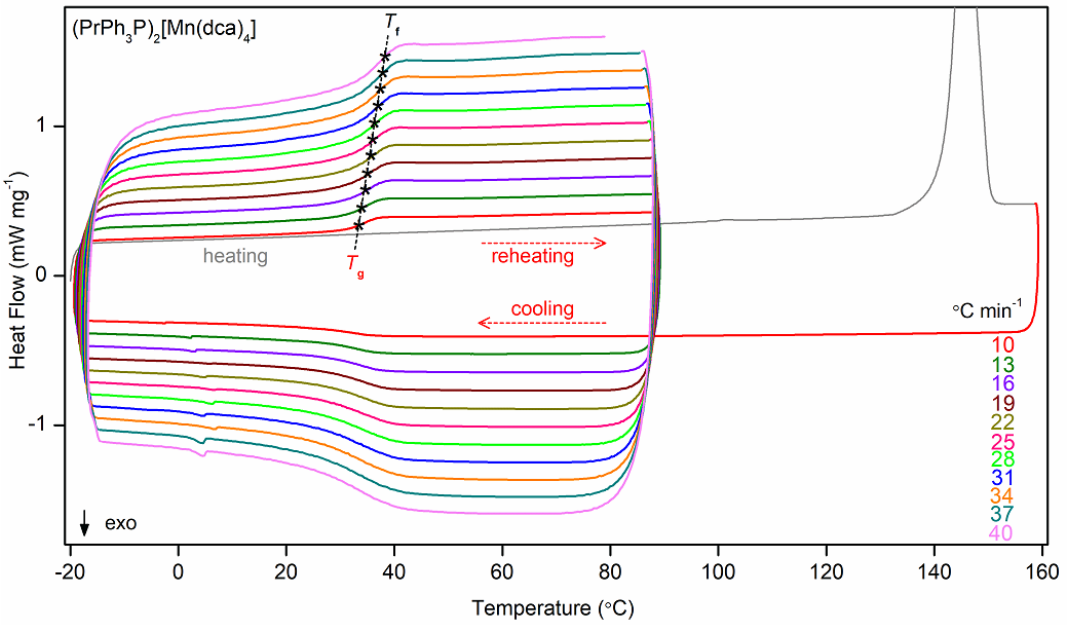

Figure S12. Dynamics of DSC cooling-reheating on $(PrPh_3P)_2[Mn(dca)_4]$ liquid at different rates, allowing determination of the fragility, *m* (as shown in **Figure 3**). The T_f (fictive temperature) and T_g (T_f at a rate of 10 °C min^{-1}) was graphically derived and marked with asterisk. Firstly, the crystalline sample is heated at 10 °C min^{-1} to the melting offset (gray color), then cooled back below room temperature to - 20 °C at 10 °C min^{-1} and then heated up to 90 °C at the same rate of 10 °C min^{-1} (red color). The liquid is then successively cooled and heated 10 times from - 20 °C to 90 °C (110 °C window) at the cooling/heating rate of 13 to 40 °C min^{-1} with an increase of cooling/heating rate by 3 °C min^{-1} each time.

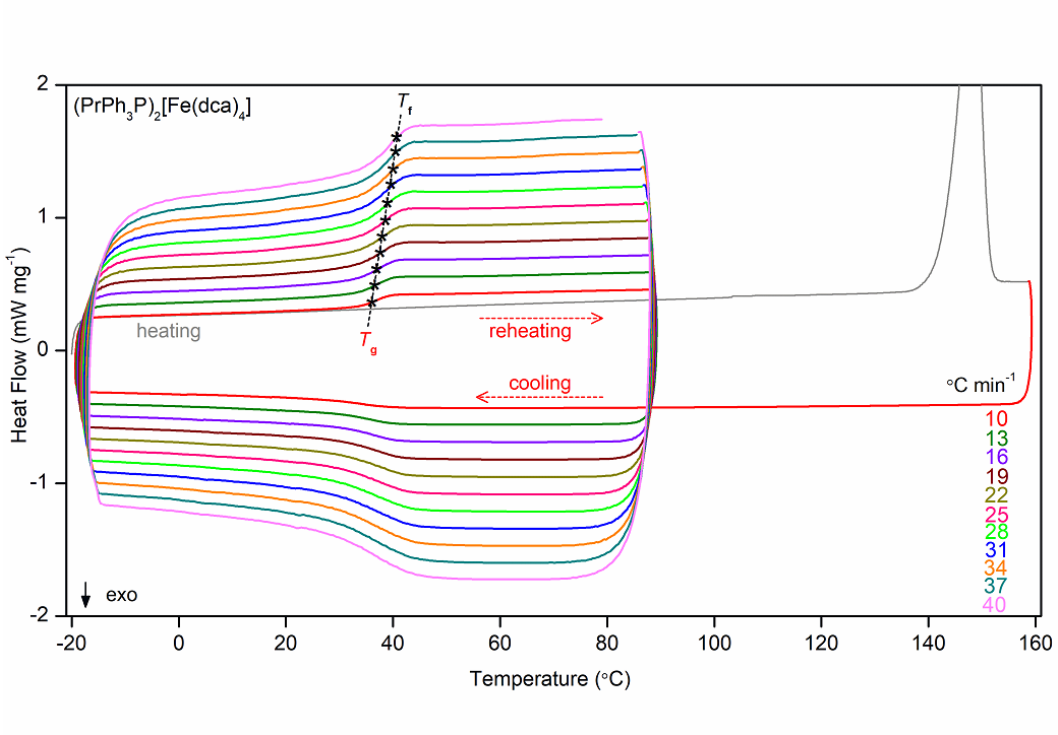

Figure S13. Dynamics of DSC cooling-reheating on $(PrPh_3P)_2[Fe(dca)_4]$ liquid at different rates, allowing determination of the fragility, *m* (as shown in **Figure 3**). The T_f (fictive temperature) and T_g (T_f at a rate of 10 °C min^{-1}) was graphically derived and marked with asterisk. Firstly, the crystalline sample is heated at 10 °C min^{-1} to the melting offset (gray color), then cooled back below room temperature to - 20 °C at 10 °C min^{-1} and then heated up to 90 °C at the same rate of 10 °C min^{-1} (red color). The liquid is then successively cooled and heated 10 times from - 20 °C to 90 °C (110 °C window) at the cooling/heating rate of 13 to 40 °C min^{-1} with an increase of cooling/heating rate by 3 °C min^{-1} each time.

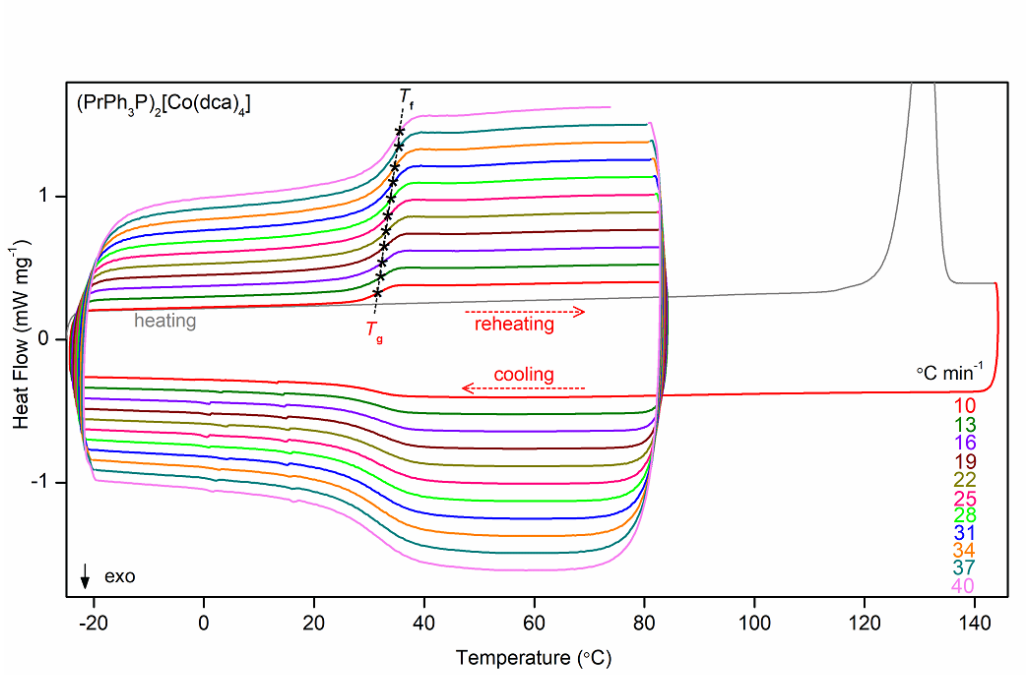

Figure S14. Dynamics of DSC cooling-reheating on $(PrPh_3P)_2[Co(dca)_4]$ liquid at different rates, allowing determination of the fragility, *m* (as shown in **Figure 3**). The T_f (fictive temperature) and T_g (T_f at a rate of 10 °C min^{-1}) was graphically derived and marked with asterisk. Firstly, the crystalline sample is heated at 10 °C min^{-1} to the melting offset (gray color), then cooled back below room temperature to - 25 °C at 10 °C min^{-1} and then heated up to 85 °C at the same rate of 10 °C min^{-1} (red color). The liquid is then successively cooled and heated 10 times from - 25 °C to 85 °C (110 °C window) at the cooling/heating rate of 13 to 40 °C min^{-1} with an increase of cooling/heating rate by 3 °C min^{-1} each time.

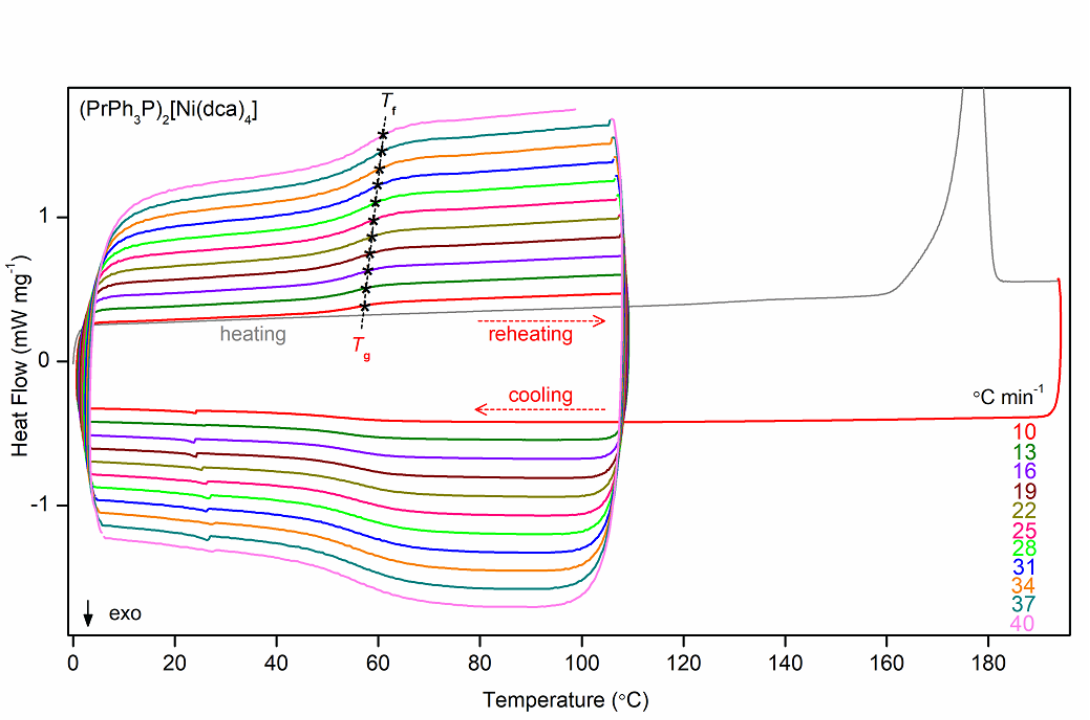

Figure S15. Dynamics of DSC cooling-reheating on $(PrPh_3P)_2[Ni(dca)_4]$ liquid at different rates, allowing determination of the fragility, *m* (as shown in **Figure 3**). The T_f (fictive temperature) and T_g (T_f at a rate of 10 °C min^{-1}) was graphically derived and marked with asterisk. Firstly, the crystalline sample is heated at 10 °C min^{-1} to the melting offset (gray color), then cooled back below room temperature to 0 °C at 10 °C min^{-1} and then heated up to 110 °C at the same rate of 10 °C min^{-1} (red color). The liquid is then successively cooled and heated 10 times from 0 °C to 110 °C (110 °C window) at the cooling/heating rate of 13 to 40 °C min^{-1} with an increase of cooling/heating rate by 3 °C min^{-1} each time.

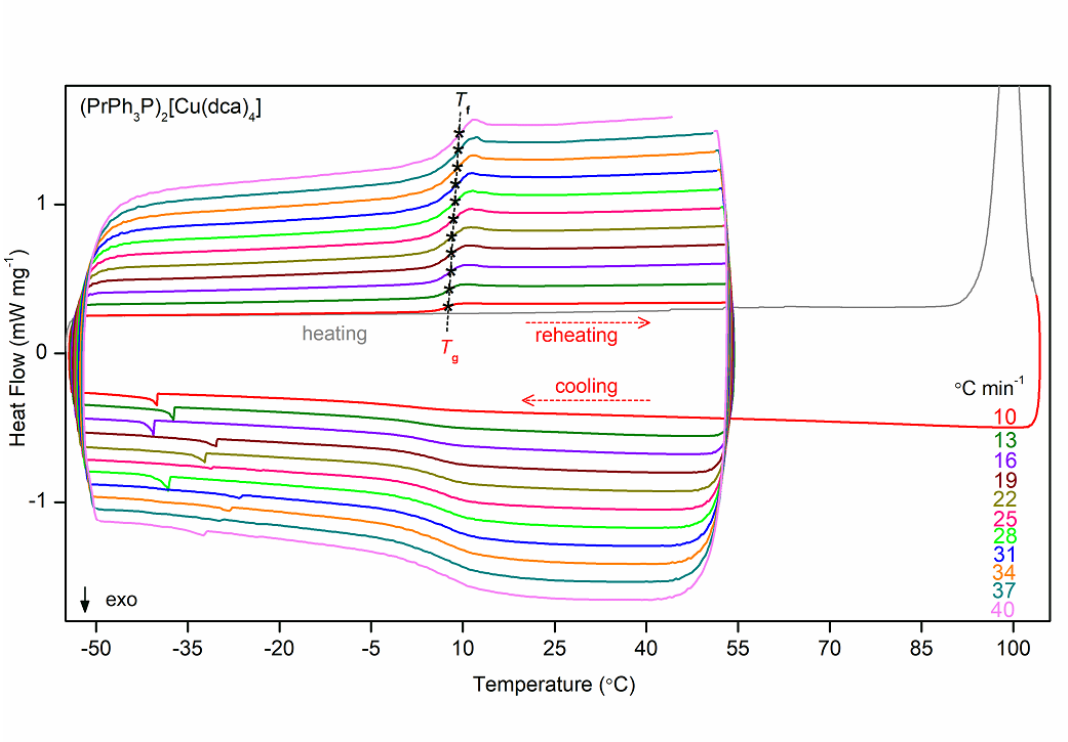

Figure S16. Dynamics of DSC cooling-reheating on $(PrPh_3P)_2[Cu(dca)_4]$ liquid at different rates, allowing determination of the fragility, *m* (as shown in **Figure 3**). The T_f (fictive temperature) and T_g (T_f at a rate of 10 °C min^{-1}) was graphically derived and marked with asterisk. Firstly, the crystalline sample is heated at 10 °C min^{-1} to the melting offset (gray color), then cooled back below room temperature to - 55 °C at 10 °C min^{-1} and then heated up to 55 °C at the same rate of 10 °C min^{-1} (red color). The liquid is then successively cooled and heated 10 times from - 55 °C to 55 °C (110 °C window) at the cooling/heating rate of 13 to 40 °C min^{-1} with an increase of cooling/heating rate by 3 °C min^{-1} each time.

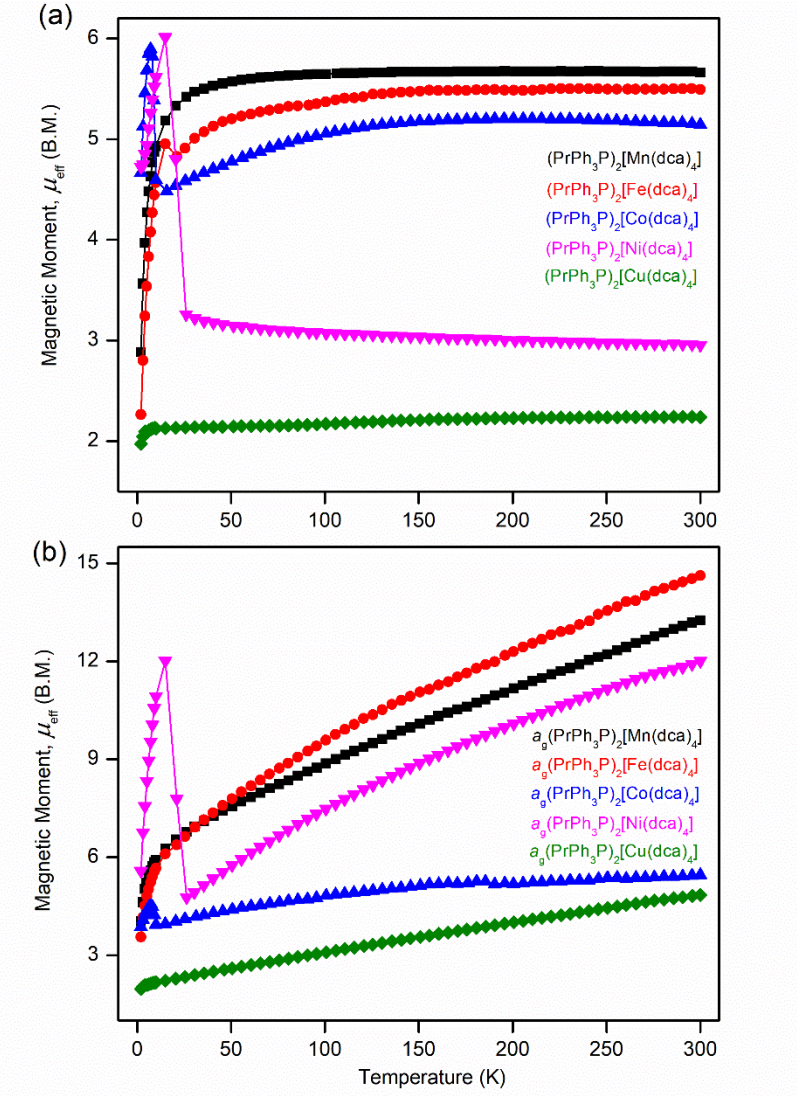

Figure S17: Variation of magnetic susceptibility in the form of effective magnetic moment (μ_{eff}) vs. temperature for (**a**) crystalline and (**b**) glass samples of $(PrPh_3P)_2[M(dca)_4]$ (where M = Mn, Fe, Co, Ni, Cu). A 100 Oe magnetic field was applied to measure the field-cooled susceptibility data.

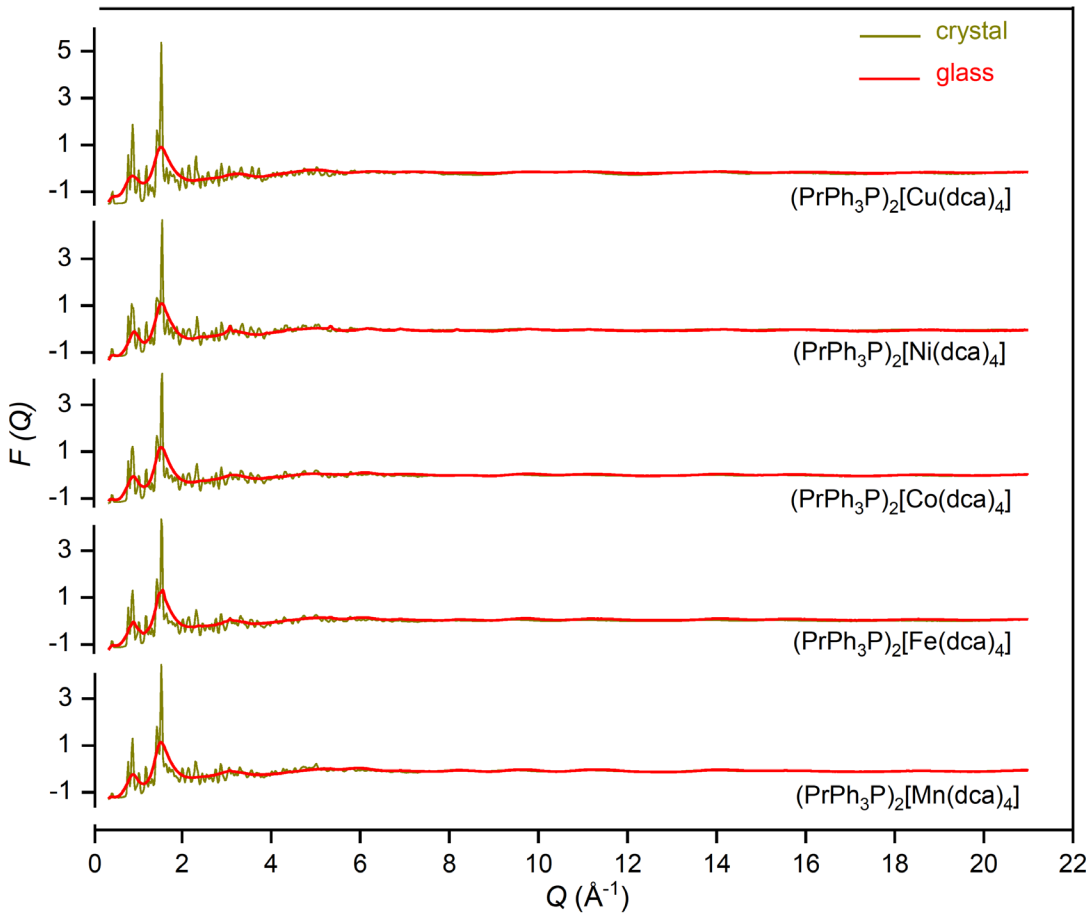

Figure S18: Room temperature X-ray total scattering data for $(PrPh_3P)_2[M(dca)_4]$ and $a_g(PrPh_3P)_2[M(dca)_4]$ (M = Mn, Fe, Co, Ni, Cu). Structure factors, $F(Q)$, of the samples before heating (dark yellow - crystal) and upon melt-quenching (red - glass).

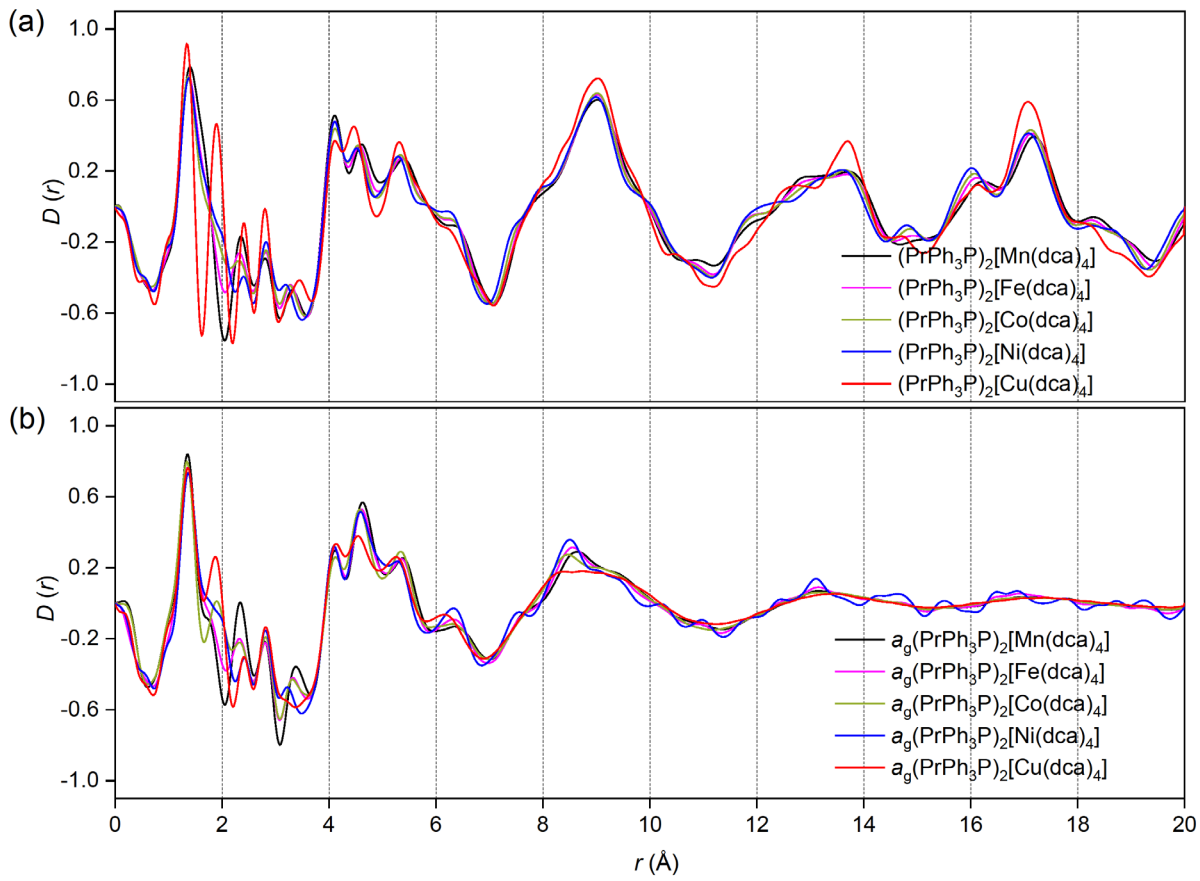

Figure S19: Pair distribution functions, $D(r)$, for (**a**) $(PrPh_3P)_2[M(dca)_4]$ crystals and (**b**) $a_g(PrPh_3P)_2[M(dca)_4]$ glasses.

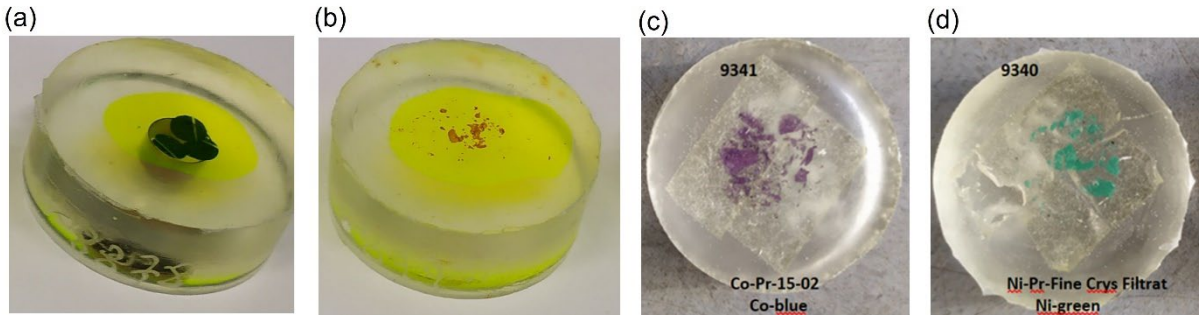

Figure S20: Glass samples of **(a)** $a_g(PrPh_3P)_2[Mn(dca)_4]$, **(b)** $a_g(PrPh_3P)_2[Fe(dca)_4]$, **(c)** $a_g(PrPh_3P)_2[Co(dca)_4]$, **(d)** $a_g(PrPh_3P)_2[Ni(dca)_4]$ are embedded in white epoxy resin for Nanoindentation experiments. The yellow coating is applied on light-colored Mn-(transparent) and Fe-(pale yellow) glass embedded samples to view properly.

Table S2. Elemental composition (C, H, N, P) of $(PrPh_3P)_2[M(dca)_4]$ (where M = Mn, Fe, Co, Ni, Cu) structures in their crystalline and glassy (a_g) states.

Samples	C	H	N	P	C-a_g	H-a_g	N-a_g	P-a_g
$(PrPh_3P)_2[Mn(dca)_4]$	63.73 (64.50)	4.75 (4.70)	18.06 (18.10)	6.80 (6.70)	63.76	4.63	17.75	7.10
$(PrPh_3P)_2[Fe(dca)_4]$	64.42 (64.50)	4.62 (4.70)	18.47 (18.10)	6.70 (6.70)	63.50	4.70	17.65	7.00
$(PrPh_3P)_2[Co(dca)_4]$	63.31 (64.50)	4.75 (4.70)	18.05 (18.10)	6.80 (6.70)	63.30	4.68	17.54	7.00
$(PrPh_3P)_2[Ni(dca)_4]$	64.70 (64.50)	4.64 (3.67)	18.49 (18.10)	6.70 (6.70)	63.22	4.67	17.69	6.90
$(PrPh_3P)_2[Cu(dca)_4]$	63.15 (64.50)	4.57 (4.70)	18.01 (18.10)	6.60 (6.70)	62.19	4.54	18.05	6.30

* Expected elemental compositions of the crystalline states were shown inside the first bracket.

Table S3. Pycnometric densities of $(PrPh_3P)_2[M(dca)_4]$ (where M = Mn, Fe, Co, Ni, Cu) structures in their crystalline (ρ_c) and glassy (ρ_g) states, and the respective glass-crystal network density deficit $\Delta\rho/\rho_g$.

Samples	ρ_c (g cm^{-3})	ρ_g (g cm^{-3})	$(\Delta\rho/\rho_g)_{network}$[a]
$(PrPh_3P)_2[Mn(dca)_4]$	1.4216 (±0.0002)	1.4485 (±0.003)	0.018
$(PrPh_3P)_2[Fe(dca)_4]$	1.6849 (±0.0003)	1.7055 (±0.0003)	0.012
$(PrPh_3P)_2[Co(dca)_4]$	1.1653 (±0.0003)	1.1784 (±0.0003)	0.011
$(PrPh_3P)_2[Ni(dca)_4]$	1.4252 (±0.0002)	1.4454 (±0.0002)	0.014
$(PrPh_3P)_2[Cu(dca)_4]$	1.5291 (±0.004)	1.5541 (±0.004)	0.016

[a] $(\Delta\rho/\rho_g)_{network} = (\rho_g - \rho_c)/\rho_g$

References

[1] *APEX4 Suite of Crystallographic Software, Version 2021-10.0,* Bruker AXS Inc., Madison, Wisconsin, USA, **2021**.

[2] Bruker, *SAINT*, *V8.40B*, Bruker AXS Inc., Madison, Wisconsin, USA.

[3] L. Krause, R. Herbst-Irmer, G. M. Sheldrick, D. Stalke, *J. Appl. Cryst.* **2015**, *48*, 3–10.

[4] G. M. Sheldrick, *Acta Cryst.* **2015**, *A71*, 3–8.

[5] G. M. Sheldrick, *Acta Cryst.* **2015**, *C71*, 3–8.

[6] C. B. Huebschle, G. M. Sheldrick, B. Dittrich, *J. Appl. Cryst.* **2011**, *44*, 1281–1284.

[7] Ed. E. Prince, *International Tables for Crystallography Volume C, Mathematical, Physical and Chemical Tables*, International Union of Crystallography, Chester, England, **2006**, 500–502; 219–222; 193–199.

[8] C. R. Groom, I. J. Bruno, M. P. Lightfoot, S. C. Ward, *Acta Cryst.* **2016**, *B72*, 171–179.